AIP Publishing

This manuscript was accepted by Appl. Phys. Lett. Click here to see the version of record.

Phonon localization transition in relaxor ferroelectric PZN-5%PT

M. E. Manley[1*], A. D. Christianson[2], D. L. Abernathy[2], R. Sahul[3]

[1]*Materials Science and Technology Division, Oak Ridge National Laboratory, Oak Ridge, Tennessee 37831, USA*
[2]*Quantum Condensed Matter Division, Oak Ridge National Laboratory, Oak Ridge, Tennessee 37831, USA*
[3]*Meggitt Sensing Systems, Irvine, CA 92606, USA*

Relaxor ferroelectric behavior occurs in many disordered ferroelectric materials, but is not well understood at the atomic level. Recent experiments and theoretical arguments indicate that Anderson localization of phonons instigates relaxor behavior by driving the formation of polar nanoregions (PNRs). Here, we use inelastic neutron scattering to observe phonon localization in relaxor ferroelectric PZN-5%PT ($0.95[Pb(Zn_{1/3}\ Nb_{2/3})O_3]$–$0.05PbTiO_3$) and detect additional features of the localization process. In the lead up to phonon localization on cooling, the local resonant modes that drive phonon localization increase in number. The increase in resonant scattering centers is attributed to a known increase in the number of locally off centered Pb atoms on cooling. The transition to phonon localization occurs when these random scattering centers increase to a concentration where the Ioffe-Regel criterion is satisfied for localizing the phonon. We also model the effects of damped mode coupling on the observed phonons and phonon localization structure.

ACCEPTED MANUSCRIPT

* manleyme@ornl.gov

AIP Publishing

This manuscript was accepted by Appl. Phys. Lett. Click here to see the version of record.

Recent theoretical[1, 2] and experimental[3] work suggests that Anderson localization of phonons initiates relaxor ferroelectric behavior by driving the formation of polar nanoregions (PNRs)[4]. It has long been known that conventional ferroelectric transitions are controlled by a soft phonon, where a zone center transverse optic (TO) phonon slows and "freezes" in the ferroelectric atomic displacements[5, 6]. Relaxor ferroelectric behavior and PNRs can emerge in ferroelectric materials when disorder is present[7-9]. Anderson localization describes the mechanism by which waves become spatially localized by constructive interference in disorder-scattered waves[10]. Although first described to explain the localization of electron wave functions[11], Anderson localization has been extended to other types of waves, including phonons[10]. Given that ferroelectric atomic displacements are controlled by phonons[5, 6] and that ferroelectric displacements become spatially localized as PNRs in the presence of disorder, Anderson localization is a natural consideration.

Anderson localization applied to relaxor ferroelectrics has emerged only recently. First-principle simulations by Akbarzadeh *et al.*[1] first suggested the possibility that Anderson localization drives PNRs. Sherrington expanded on this by showing that equations used to describe relaxor ferroelectric behavior can be mapped onto the Anderson localization problem[2]. Experimental evidence of Anderson localized phonons was found using inelastic neutron scattering by Manley *et al.*[3] in a search for intrinsic localized modes[12-14] in PMN-30%PT ($0.7[Pb(Mg_{1/3}Nb_{2/3})O_3]$–$0.3PbTiO_3$). Intrinsic localized modes had been proposed as a mechanism for PNRs[15-17], but the theory did not match the modes observed[3]. The stability of intrinsic localized modes is predicated on the idea that nonlinearity shifts a local vibration out of the normal phonon spectrum, where it exists out of resonance with phonons[13]. Localization in PMN-30%PT occurs in the phonon bands and with characteristics matching Anderson localized transverse optic (TO) phonons[3]. Local resonant modes, attributed to local Pb atom off centering[3, 18, 19], provide the random scattering centers driving nanoscale localization[10].

Here, we demonstrate phonon localization in PZN-5%PT. On cooling below the Burns temperature[4], local (atomic) resonant modes first increase in number, followed by an abrupt increase in intensity and a shift of local mode intensity towards the ferroelectric TO phonon, signifying a transition to nanoscale localization. In previous experiments[3] too

ACCEPTED MANUSCRIPT

AIP Publishing

This manuscript was accepted by Appl. Phys. Lett. Click here to see the version of record.

few temperatures were measured to observe this increase in resonance modes. The transition to phonon localization occurs when these random scattering centers reach a critical density on cooling set by the Ioffe-Regel condition[10]. This increase in scattering centers is attributed to an increase in locally off centered Pb atoms below the Burns temperature[20]. The phonon-localization temperature corresponds to an intermediate temperature associated with an elastic component of the PNR diffuse scattering[21]. This elastic diffuse scattering indicates PNRs "freezing" well below the Burns temperature. PNR diffuse scattering that appears above this temperature is quasielastic and exhibits diffusion[21]. The halting of the diffusive motion of the PNRs is reminiscent of the halting of electron diffusion in Anderson's original work[11]. Slow diffusing PNRs just prior to localization are consistent with weak localization, a precursor to Anderson localization[10]. It has been argued that the Burns temperature should be redefined to the lower PNR "freezing" temperature[22]. Here, both temperatures have meaning; the Burns temperature the onset of weak localization and the PNR freezing temperature the onset of Anderson localization. While the phonon localization appears similar to PMN-30%PT[3], mode damping is larger in PZN-5%PT, and this requires a coupled-damped harmonic oscillator model[23] to fully explain.

A ~10 cm^3 single crystal of PZN-5%PT was measured on the HB3 spectrometer at the High Flux Isotope Reactor at Oak Ridge National Laboratory (ORNL). The spectrometer was operated with pyrolitic graphite filtered fixed final neutron energy of 14.7 meV with horizontal collimation 48': 60': 80': 120', and the instrument used pyrolitic graphite PG(002) for the monochromator and analyzer. The crystals were mounted in a furnace with the (HK0) reflections in the scattering plane in a vanadium holder. Measurements were made along $\boldsymbol{Q}$ = [2, K, 0] at 21 equally spaced values of K between 0 and 0.5 at four temperatures above the Curie temperature (T_C = 425 K): 500 K, 688 K, 788 K, and 888 K. The strong Bragg extinction indicates a crystal mosaic of < 0.038° above T_C, and results in Bragg-phonon multiple scattering processes that are of order ~ 0.2% of a normal phonon, which is much less than the intensity of the observed local mode. Time-of-flight measurements were performed on the same crystal using the Angular-Range Chopper Spectrometer (ARCS) at the Spallation Neutron Source of ORNL[24] at 688 K with the crystals oriented in the (HK0) plane and with incident neutron

ACCEPTED MANUSCRIPT

AIP Publishing

This manuscript was accepted by Appl. Phys. Lett. Click here to see the version of record.

energy of 25 meV. Rotating the angle between the crystal [100] axis and the incident beam from 0 to 60 degrees in 0.5-degree steps and combining the data[25] provides comprehensive ***Q***-*E* volumes of data.

The PZN-5%PT single crystal was cut from a boule grown using a modified Bridgman growth method. The boule was oriented using a Laue X-ray diffractometer. The composition of the crystal used in the measurements was confirmed by measuring the transition temperature using high-temperature x-ray diffraction.

The mode-coupling model includes coupled damped harmonic oscillators representing the TO and transverse acoustic (TA) modes, plus an uncoupled local mode (LM). LM is used as the generic label for both the resonant local mode (atomic) and the Anderson localized TO phonon (nanoscale), with the distinction being the intensity profile. The dynamical matrix, $\mathbf{D}_q$, is defined as[23, 26],

$$\mathbf{D}_q = \begin{pmatrix} \omega_{\mathrm{TA}}^2(q) & 0 & \Delta(q) \\ 0 & \omega_{\mathrm{LM}}^2 & 0 \\ \Delta(q)^* & 0 & \omega_{\mathrm{TO}}^2(q) \end{pmatrix}, \tag{1}$$

where $\omega_{TA}(q)$, ω_{LM}, and $\omega_{TO}(q)$ represent the bare dispersion curves, with q the phonon wavevector. The local mode energy, ω_{LM}, is matched to the experiment at 10.6 meV. The off diagonal term, $\Delta(q)$, describes the interaction between the TA and TO modes. The damping matrix is

$$\mathbf{\Gamma}_q = \begin{pmatrix} \Gamma_{\mathrm{TA}}(q) & 0 & 0 \\ 0 & \Gamma_{\mathrm{LM}}(q) & 0 \\ 0 & 0 & \Gamma_{\mathrm{TO}}(q) \end{pmatrix}, \tag{2}$$

where $\Gamma_{\mathrm{TA}}(q)$, $\Gamma_{\mathrm{LM}}(q)$, and $\Gamma_{\mathrm{TO}}(q)$ are the bare mode frequency independent damping. As in Ref. [23] the off-diagonal terms are assumed to be negligible. The inelastic neutron scattering spectrum in the high temperature limit ($kT >> \hbar\omega$) is

$$I(\omega, q) = kT\omega^{-1}\mathbf{f}(q)^*\mathrm{Im}[\mathbf{G}(\omega, q)]\mathbf{f}(q), \tag{3}$$

$$\mathbf{G}(\omega, q) = (\mathbf{D}_q - i\omega\mathbf{\Gamma}_q - \omega^2\mathbf{E})^{-1}, \tag{4}$$

where $\mathbf{E}$ is a 3×3 unit matrix and $\mathbf{f}(q) = \begin{pmatrix} 0.6 \\ 0.06 \\ 0.5 \end{pmatrix}$ is a vector characterizing the structure factors of the bare modes. The bare dispersion curves are given by[23]

$$\omega_{TA}^2(q) = A\sin^2(\pi q), \tag{5}$$

ACCEPTED MANUSCRIPT

AIP Publishing

This manuscript was accepted by Appl. Phys. Lett. Click here to see the version of record.

$$\omega_{TO}^2(q) = B + C\sin^2(\pi q), \quad (6)$$

$$\Delta(q) = d\sin^2(\pi q), \quad (7)$$

where A = 100 meV^2, B = 90 meV^2, and C = 100 meV^2 define the strength of the dispersion and d = 100 meV^2 defines the strength of the mode mixing[23]. The bare mode independent damping terms are defined as[23] $\Gamma_{\mathrm{TA}}(q) = g\sin^2(\pi q)$, $\Gamma_{\mathrm{LM}}(q) = h$, $\Gamma_{\mathrm{TO}}(q) = l$, where g = 4 meV, h = 1 meV, and l = 5 meV. The functional forms used for the mode mixing parameter and the TA mode damping parameter are chosen to give the correct asymptotic behavior for q ➔ 0 [23].

Figure 1 shows the phonon dispersion curves measured along $\boldsymbol{Q}$ = [2, K, 0], which probes transverse modes. The TO and TA phonons are strongly damped. The LM dispersion, which is nearly flat at all temperatures from 888 K (Fig. 1(a)) down to 500 K (Fig. 1(d)), shows a slight softening in cooling from 888 K (Fig. 1(c)) to 500 K (Fig. 1(d)), where it decreases from 10.9±0.1 meV to 10.6±0.1 meV. Peak positions are determined by fitting the peaks to three Lorentzian functions. There is also a more complete flattening of the LM dispersion at 500 K, which is indicative of localization. At the higher temperatures the LM bends slightly near TO phonon in an expected avoided crossing[27, 28]. Similar to PMN-30%PT[3], there is a dramatic increase in the LM intensity towards the LM-TO intersection near 500 K, as deduced from the fits to the neutron scattering intensities (see fits to data in right panels in Fig. 1). The change in the LM intensity profile indicates a transition to nanoscale phonon localization.

Figure 2 shows the transition to phonon localization for in the LM intensity profile. Figure 2(a) shows example fits to the inelastic neutron scattering profiles using Lorentzian functions at K = 0.3, 0.35, 0.45 above the transition to phonon localization at 688 K and below the transition at 500 K. Figure 2(b) summarizes the LM intensity profile as a function of K. For 688 K and higher the LM intensity profile is essentially flat as a function of K. This is the same behavior as the LM in PMN-30%PT, and is attributed to local resonant modes associated with Pb-atom off centering[3]. These modes are well localized to off-centered Pb atoms, analogous to resonant impurity modes[29]. As shown in Fig. 2(b) the intensity of these flat modes increases on cooling below the ~750 K Burns temperature (T_d). This is consistent with the reported increase in Pb atom off centering on cooling below T_d[19, 20] and is expected from theoretical considerations[18]. An increase in

ACCEPTED MANUSCRIPT

AIP Publishing

This manuscript was accepted by Appl. Phys. Lett. Click here to see the version of record.

resonant scattering centers leading up to localization makes sense since localization only occurs when the scattering centers become sufficiently dense to trap a phonon wavelength on the nanoscale[10]. At $K = 0.35$ for 688 K the LM intensity (integrated peak area) is 10±2% the strength of the TO phonon. Anderson localization is expected when distance between scattering centers, l, becomes comparable to the phonon wavelength, which can be expressed as the Ioffe-Regel criterion, $ql \lesssim 1$ [10]. At 10% the distance between resonant modes is about 2 lattice units (2a). Taking $K = 0.15$ in reduced lattice units (bare phonon estimate[23], see below) $q = K(2\pi/a)$, so $ql = 0.15(2\pi/a)(2a) = 1.88$, which is close to the 1.8 value found for localizing ultrasound shear waves in an elastic network[30]. At 500 K, rather than being flat, the intensity concentrates towards the LM-TO crossing. The profile is similar to that attributed to TO-phonon localization in PMN-30%PT[3].

The phonon dispersion curves shown in Fig. 3 have been extracted from the phonon peak positions measured along $\boldsymbol{Q} = [2, K, 0]$ and $\boldsymbol{Q} = [3, K, 0]$, which are equivalent locations in the crystal but have different structure factors. The solid points were measured using constant $\boldsymbol{Q}$ scans on the HB3 triple axis spectrometer (circles) or equivalently constant $\boldsymbol{Q}$ slices of the ARCS time-of-flight data (diamonds). The open symbols were extracted from constant energy slices of the ARCS data. The result for the "waterfall" effect for PZN-5%PT measured here are essentially identical to that reported for PZN-8%PT[23]. Along $\boldsymbol{Q} = [2, K, 0]$ the waterfall and descending branch of the TO phonon appear to be at slightly higher values of K than for $\boldsymbol{Q} = [3, K, 0]$, even up near 10 meV where phonon localization occurs. The TA phonon also appears to be shifted to higher energy along $\boldsymbol{Q} = [2, K, 0]$ compared to $\boldsymbol{Q} = [3, K, 0]$. The overall effect is that the TO and TA phonons appear closer together in the (200) zone, which shows a more pronounced effect of the TO-TA mode coupling[23]. The part of the TO phonon that becomes localized is determined by the intersection of the LM and the TO dispersion curves[3]. Since the intersection appears to depend on zone while the modes themselves cannot be different by symmetry, a more sophisticated approach must be taken to interpret the spectral intensities. To address this issue we apply the coupled damped harmonic oscillator approach[23].

The mode-coupling model in Fig. 4 shows the effect damped phonon coupling has on the normal phonons (Fig. 4(a)) and the phonon localization structure (Fig. 4(b)). The

ACCEPTED MANUSCRIPT

AIP Publishing

This manuscript was accepted by Appl. Phys. Lett. Click here to see the version of record.

main effect of coupling the normal phonons is a column of shared intensity extending between the TA and TO phonons[23]. To characterize the "waterfall" feature in Fig. 4(a) we plot the position of peak intensity deduced from constant energy cuts along [2, *K*, 0], as was done with the experimental "waterfall" in Fig. 3. The coupling shifts apparent the LM-TO intersection to higher values of *K*. The bare TO phonon (dashed line) crosses the LM around $K = 0.15$ compared to an apparent crossing of $K = 0.2$ (solid line), see Fig. 4(a). A lower value of *K* implies a longer wavelength for the localized TO phonons, and longer wavelengths imply larger PNRs. For PMN-30%PT the value of *K* at the LM-TO intersection is about 0.2 and this corresponds to about 2 nm, which is about the size of the PNRs in PMN-30%PT[3]. Accounting for mode coupling, the LM-TO intersection in PZN-5%PT must occur at a longer wavelength, which is qualitatively consistent with the narrower PNR diffuse scattering (larger PNRs) in PZN-PT[31]. The mode coupling correction makes it difficult to obtain a precise size for the Anderson local modes.

The ideal un-localized bare TO phonon is infinitely extended in space and time, which means sharp in both momentum and energy. A finite phonon lifetime broadens the mode in energy while spatial localization broadens the mode in momentum. For Anderson localization, the spatial localization is exponential[3, 10]. In the transformation to reciprocal space this becomes a Lorentzian broadening function in momentum. The characteristic length scale is the wavelength of the localized phonon. For PMN-30%PT the width of the LM profile in momentum gives a coherence length (size) that is equal to the localized TO phonon wavelength[3]. The bare TO phonon localization (what localization would look like without broadening/damping) shown in Fig. 4(b) meets this condition. Unlike for PMN-30%PT, however, this localization broadening is less than the inherent broadening of the observed TO phonon. In this case it is not appropriate to represent the starting TO phonon with a sharp line in momentum, but rather the broad profile of the TO phonon must be convoluted with the bare localization function. The TO profile was estimated by removing the LM from the model and then using the constant energy cut at 10.6 meV (the LM energy). The LM profile for phonon localization with mode broadening shown in Fig. 4(b) is obtained by convoluting the extracted TO profile with the bare phonon localization. This result agrees well with observed LM intensity profile for the localized phonon observed at 500 K, Fig. 4(b).

ACCEPTED MANUSCRIPT

AIP Publishing

This manuscript was accepted by Appl. Phys. Lett. Click here to see the version of record.

In his classic 1959 paper on the theory of ferroelectricity Cochran[5] concludes that, "*the onset of ferroelectric properties in any crystal is a problem in lattice dynamics*". In 1959 relaxor ferroelectric behavior[32], PNRs[4], and Anderson localized phonons[10] had not been discovered. The evidence herein of Anderson-localized phonons explains how lattice dynamics may initiate relaxor ferroelectric behavior in the presence of disorder. On cooling, the local off centering of Pb atoms[18-20] introduces an increasing number of disordered scattering centers, which manifest as resonant local modes (Figs. 1 and 2). Eventually, the density of scattering centers (resonant modes) becomes high enough to drive nanoscale localization[10] of the ferroelectric TO phonon (Fig. 2(b)). Within the Anderson localized spatial regions, the average distortion of the local structure results in the more commonly observed static component of the PNRs[20].

Mode damping originates with phonon scattering, by disorder[33] and/or anharmonic phonon-phonon interactions[34]. Strong anharmonic scattering with other phonons undermine localization by depleting the phonons before they can travel along paths to constructively interfere[10]. That localization occurs suggests that disorder scattering dominates the broadening. Disorder broadening of phonons can be constructed in a harmonic lattice by superimposing the lattice dynamical solutions for a large number of pseudo-random supercell configurations[29]. In this view, a distribution of phonon localization widths corresponds to localization varying within the different spatial regions with slightly different phonon wavelengths.

Our results support recent theoretical[1, 2] and experimental[3] arguments that Anderson localization on the nanoscale initiates relaxor behavior by driving the formation of polar nanoregions.

ACKNOWLEDGEMENTS

Research sponsored by the U.S. Department of Energy, Office of Basic Energy Sciences, Materials Sciences and Engineering Division. The research performed at the Oak Ridge National Laboratory's High Flux Isotope Reactor and Spallation Neutron Source was sponsored by the U. S. Department of Energy, Office of Basic Energy Sciences.

ACCEPTED MANUSCRIPT

AIP Publishing

This manuscript was accepted by Appl. Phys. Lett. Click here to see the version of record.

[1] A. R. Akbarzadeh, S. Prosandeev, E. J. Walter, A. Al-Barakaty, and L. Bellaiche, Phys. Rev. Lett. **108**, 257601 (2012).

[2] D. Sherrington, Phys. Rev. Lett. **111**, 227601 (2013).

[3] M. E. Manley, J. W. Lynn, D. L. Abernathy, E. D. Specht, O. Delaire, A. R. Bishop, R. Sahul, and J. D. Budai, Nat. Commun. **5**, 3683 (2014).

[4] G. Burns, and F. H. Dacol, Phys. Rev. B **28**, 2527–2530 (1983).

[5] W. Cochran, Phys. Rev. Lett. **3**, 412 (1959).

[6] P. W. Anderson, Izv. Akad. Nauk, 290 (1960).

[7] R. A. Cowley, S. N. Gvasaliya, S. G. Lushnikov, B. Roessli, and G. M. Rotaru, Adv. Phys. **60**, 229 (2011).

[8] A. E. Bokov, J. Mater. Sci. **41**, 31 (2006).

[9] G. A. Samara, J. Phys.: Condens. Matter **15**, R367 (2003).

[10] A. Lagendijk, B. van Tiggelen, D. S. Wiersma, Phys. Today **62**, 24–29 (2009).

[11] P. W. Anderson, Phys. Rev. **109**, 1492 (1958).

[12] D. K. Campbell, S. Flach, and Y. S. Kivshar, Phys. Today **57**, 43 (2004).

[13] S. Flach and A. Gorbach, *Discrete Breathers-Advances in Theory and Applications* (Elsevier Science, New York, 2008).

[14] M. E. Manley, A. J. Sievers, J. W. Lynn, S. A. Kiselev, N. I. Agladze, Y. Chen, A. Llobet, and A. Alatas, Phys. Rev. B **79**, 134304 (2009).

[15] A. Bussmann-Holder, A. R. Bishop, and T. Egami, Europhys. Lett. **71**, 249–255 (2005).

[16] A. R. Bishop, A. Bussmann-Holder, S. Kamba, and M. Maglione, Phys. Rev. B **81**, 064106 (2010).

[17] J. Macutkevic, J. Banys, A. Bussmann-Holder, and A. R. Bishop, Phys. Rev. B **83**, 184301 (2011).

[18] B. P. Burton and E. Cockayne, Phys. Rev. B **60**, R12 542 (1999).

[19] T. Egami and S. J. L. Billinge, *Underneath the Bragg Peaks Structural Analysis of Complex Materials* Ed. R. W. Cahn (Pergamon Materials Series, 2003) p. 343.

[20] W. Dmowski, S. B. Vakhrushev, I.-K. Jeong, M. P. Hehlen, F. Trouw, and T. Egami, Phys. Rev. Lett. **100**, 137602 (2008).

ACCEPTED MANUSCRIPT

AIP Publishing

This manuscript was accepted by Appl. Phys. Lett. Click here to see the version of record.

[21] G.-M. Rotaru, S. N. Gvasaliya, B. Roessli, S. Kojima, S. G. Lushnikov, and P. Gunter, Appl. Phys. Lett. **93**, 032903 (2008).

[22] P. M. Gehring, H. Hiraka, C. Stock, S.-H. Lee, W. Chen, Z.-G. Ye, S. B. Vakhrushev, and Z. Chowdhuri, Phys. Rev. B **79**, 224109 (2009).

[23] J. Hlinka, S. Kamba, J. Petzelt, J. Kulda, C. A. Randall, and S. J. Zhang Phys. Rev. Lett. **91**, 107602 (2003).

[24] D. L. Abernathy, M. B. Stone, M. J. Loguillo, M. S. Lucas, O. Delaire, X. Tang, J. Y.Y. Lin, and B. Fultz, Rev. of Sci. Instr. **83**, 15114 (2012).

[25] R. T. Azuah, L. R. Kneller, Y. Qiu, P.W.W. Tegenna-Piggott, C.M. Brown, J.R.D. Copley, and R.M. Dimeo, J. Res. Natl. Inst. Stan. Technol. **114**, 341 (2009).

[26] M. E. Manley, D. L. Abernathy, R. Sahul, P. J. Stonaha, and J. D. Budai, *Phys. Rev. B* **94**, 104304 (2016).

[27] B. Skinner, *There's nothing particularly "spooky" about avoided crossing,* https://gravityandlevity.wordpress.com/2014/04/08/avoided-crossing/, accessed, May, (2016).

[28] M. E. Manley, D. L. Abernathy, R. Sahul, D. E. Parshall, J. W. Lynn, A. D. Christianson, P. J. Stonaha, E. D. Specht, J. D. Budai, *Science Adv.* **2**, e1501814 (2016).

[29] O. Delaire, I. I. Al-Qasir, A. F. May, C. W. Li, B. C. Sales, J. L. Niedziela, J. Ma, M. Matsuda, D. L. Abernathy, and T. Berlijn, Phys. Rev. B **91**, 094307 (2015).

[30] H. Hu, A. Strybulevych, J. H. Page, S. E. Skipetrov, and B. A. van Tiggelen, *Nature Phys.* **4**, 945 (2008).

[31] P. M. Gehring, S.-E. Park, and G. Shirane, Phys. Rev. Lett. **84**, 5216–5219 (2000).

[32] G. A. Smolenskii, V. A. Isupov, A. I. Agranovskaya, and S. N. Popov, Sov. Phys. Solid State **2**, 2584 (1961).

[33] R. A. Cowley, Rep. Prog. Phys. **31**, 123 (1968).

[34] A. Gobel, D. T. Wang, M. Cardona, L. Pintschovius, W. Reichardt, J. Kulda, N. M. Pyka, K. Itoh, E. E. Haller, Phys. Rev. B **58**, 10510 (1998).

ACCEPTED MANUSCRIPT

AIP Publishing

This manuscript was accepted by Appl. Phys. Lett. Click here to see the version of record.

Figure Captions

FIG. 1. Triple-axis inelastic neutron scattering measurements of the phonon dispersion along $\boldsymbol{Q}$ = [2, K, 0] in PZN-5%PT as a function of temperature. Right hand panels show examples of fits to data used to determine the dispersion data points overlaying the intensity dispersion maps (data sets are offset for clarity). At all temperatures there is a local mode (LM), a transverse acoustic (TA) phonon, and a transverse optic (TO) phonon. (a) Shows measurements above the conventional Burns temperature (T_d ~ 750 K) at 888 K, (b) shows near T_d, while (c) and (d) are measured between T_d and the Curie temperature (T_C ~ 415 K). However, (d) is measured near the so-called revised lower Burns temperature (T^* ~ 500 K) associated with the freezing in of static polar nanoregions [21, 22]. The extra weak features highlighted in blue in (c) and (d) are probably associated with the being near the leading edge of "waterfall" effect, in which intensity extends in a vertical column between the TO and TA phonons at lower values of K [3, 23, 29]. Data were collected on the HB3 triple-axis spectrometer at the High Flux Isotope Reactor (HFIR) at Oak Ridge National Laboratory.

FIG. 2. Intensity profile of the local mode (LM) as a function of position in the (200) zone along $\boldsymbol{Q}$ = [2, K, 0] in PZN-5%PT as a function of temperature. (a) Shows fits to the data at a few K points above and below the transition to phonon localization, see text for details. (b) The deduced LM intensities as a function of K for all temperatures measured. For 688 K and above the intensity appears nearly flat and a straight line has been fit to each temperature. At 500 K the intensity becomes strongly peaked near the TO-LM intersection, as expected with TO phonon localization [3].

FIG. 3. Phonon dispersion curves deduced from measurements along $\boldsymbol{Q}$ = [2, K, 0] and $\boldsymbol{Q}$ = [3, K, 0] in PZN-5%PT at 688 K. The solid symbols where determined by fitting peaks observed in constant $\boldsymbol{Q}$ cuts. The open symbols where determined by fitting peaks observed in constant energy cuts. The circle symbols are from data collected on the HB3 triple-axis spectrometer at the High Flux Isotope Reactor (HFIR) at Oak Ridge National Laboratory. The diamond symbols are from data collected on the ARCS spectrometer at

ACCEPTED MANUSCRIPT

AIP Publishing

This manuscript was accepted by Appl. Phys. Lett. Click here to see the version of record.

the Spallation Neutron Source (SNS) at Oak Ridge National Laboratory. The differences between (200) and (300) zones are a consequence of damped mode coupling [23].

FIG. 4. Results of a damped mode-coupling model used to describe the phonon structure, and the phonon-localization structure observed in PZN-5%PT. (a) Damped mode coupling model intensities. The bare TO is the dispersion curve without mode coupling. The "waterfall" feature is obtained using the same procedure applied to the data, which is to plot the peak positions in constant energy slices. The damped mode coupling has the effect of making TO-LM intersection appear to be at a higher value of K. (b) The LM intensity profile for bare TO phonon localization and phonon localization with mode broadening, see text for details. The measured data points from Fig. 2(b) are repeated here (symbols).

ACCEPTED MANUSCRIPT

This manuscript was accepted by Appl. Phys. Lett. Click here to see the version of record.

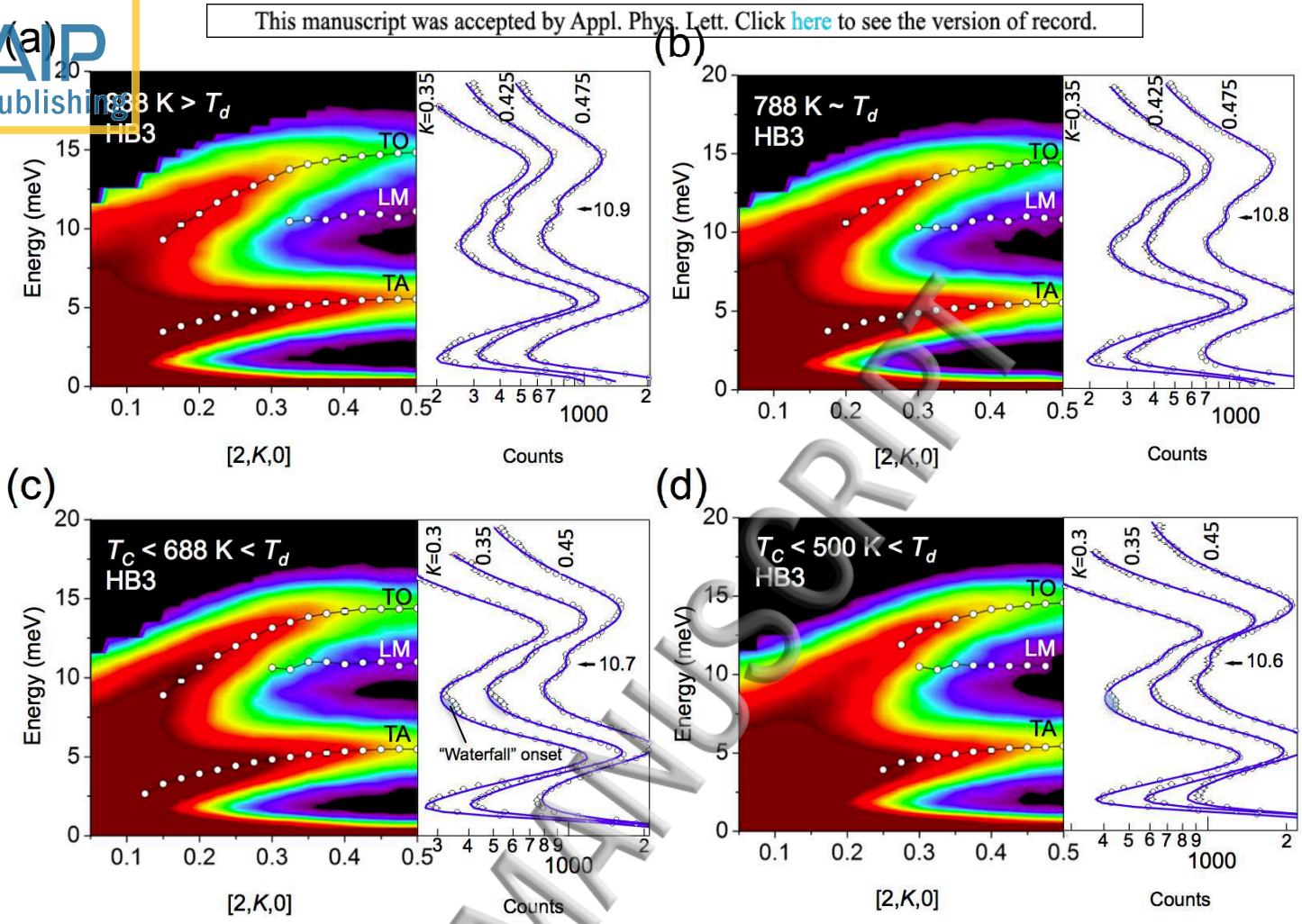

ACCEPTED MANUSCRIPT

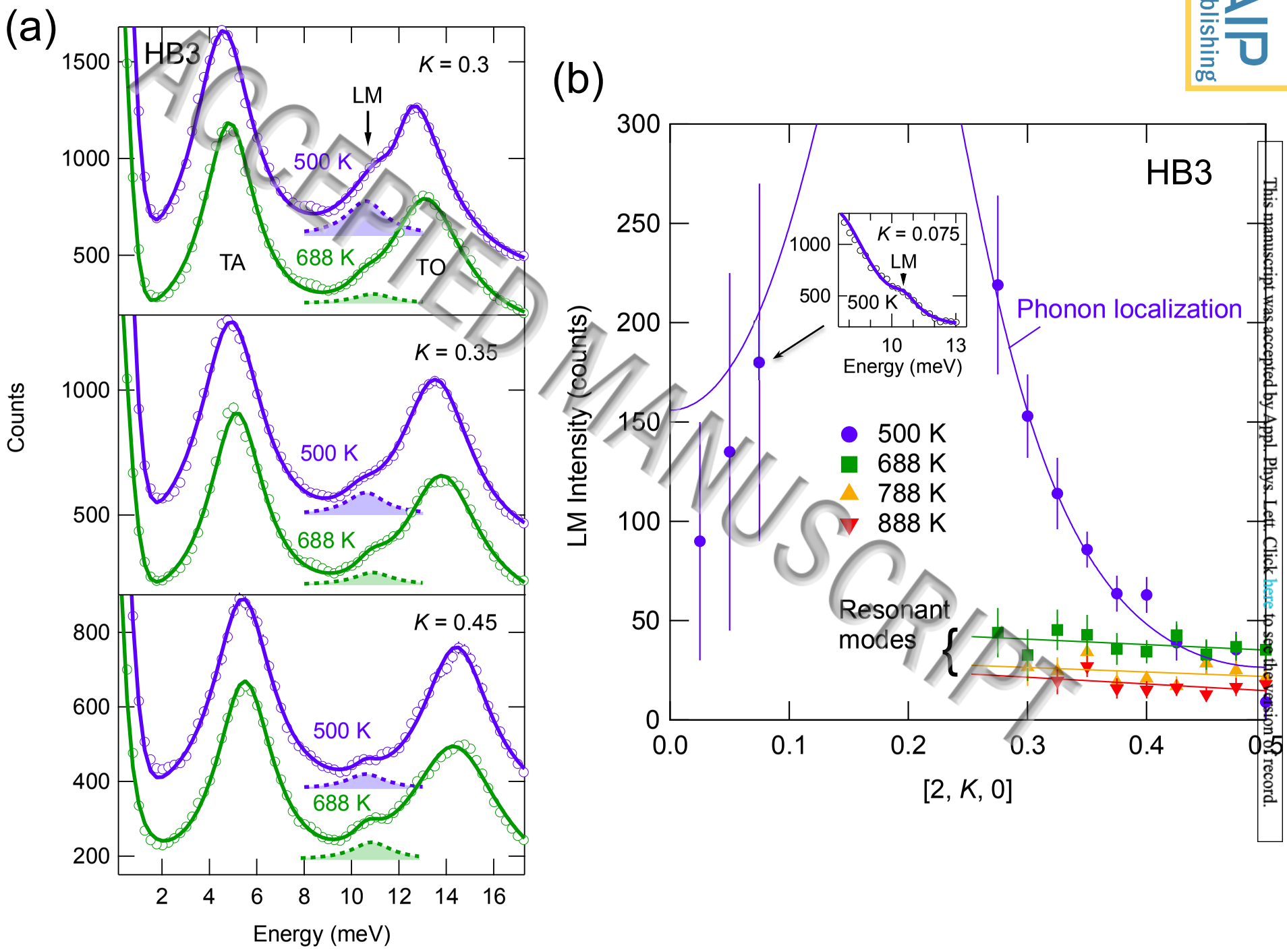

ACCEPTED MANUSCRIPT

This manuscript was accepted by Appl. Phys. Lett. Click here to see the version of record.

AIP Publishing

AIP Publishing

This manuscript was accepted by Appl. Phys. Lett. Click here to see the version of record.

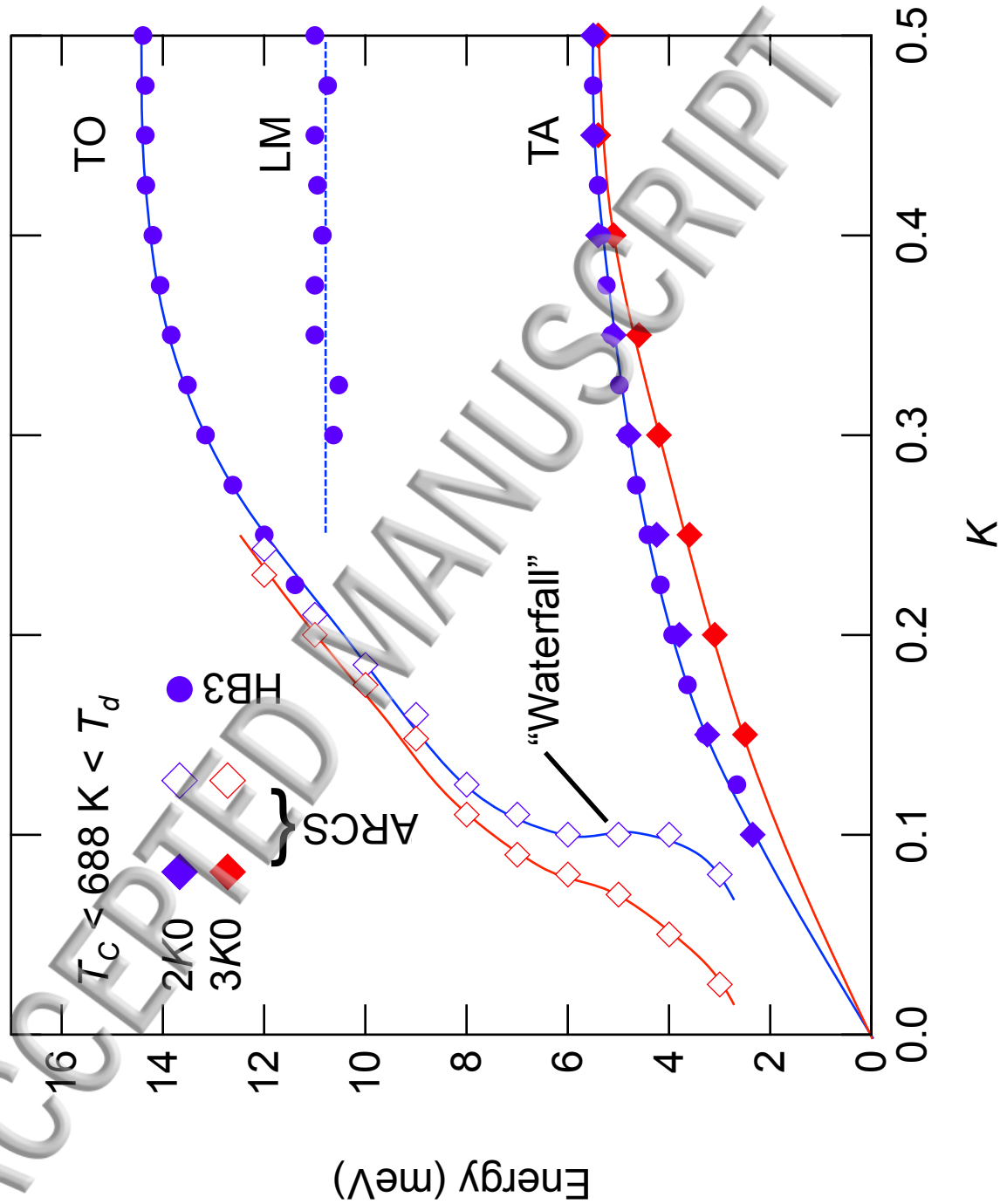

ACCEPTED MANUSCRIPT

This manuscript was accepted by Appl. Phys. Lett. Click here to see the version of record.

(a)

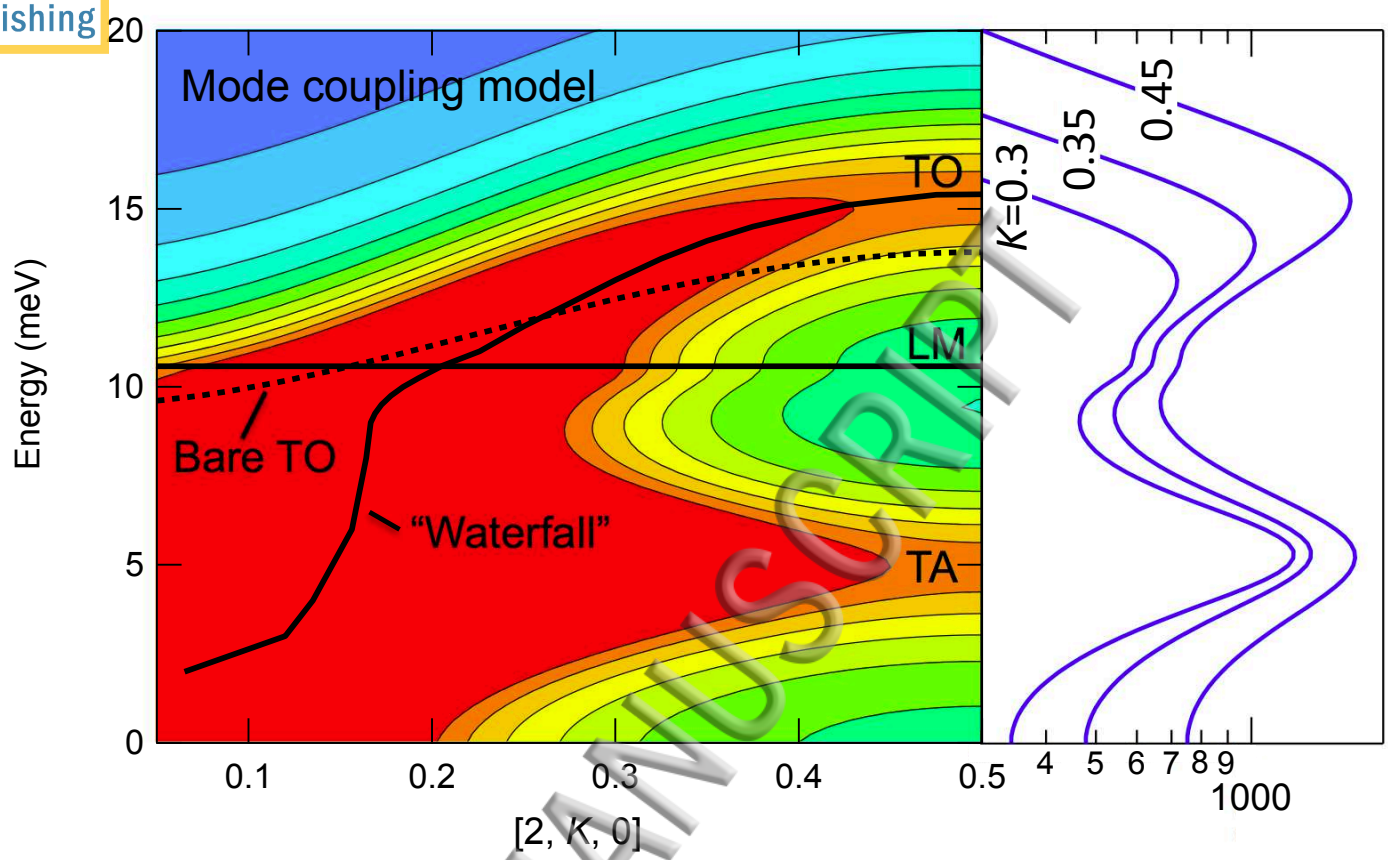

(b)

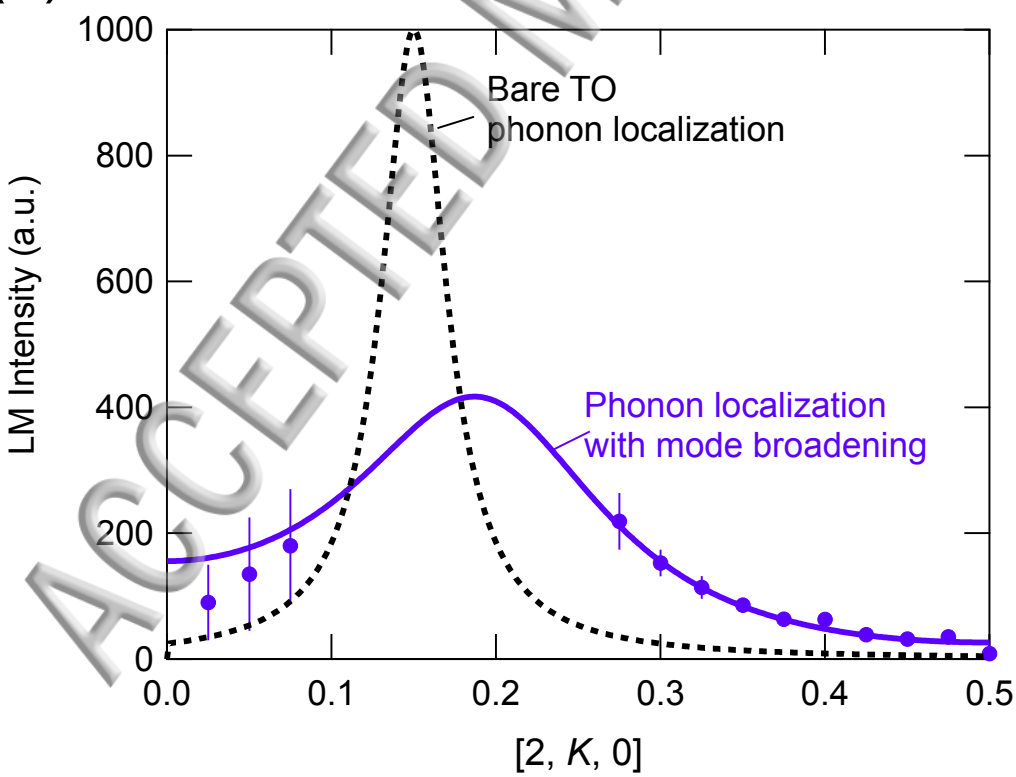

ACCEPTED MANUSCRIPT